


Article

Structural Variations across Wolframite Solid Solutions, (Fe,Mn)WO₄

Darren A. Umbsaar and Styte M. Antao * 

Department of Geoscience, University of Calgary, Calgary, AB T2N 1N4, Canada; daumbsaa@ucalgary.ca

* Correspondence: antao@ucalgary.ca

Abstract: The crystal structure of four samples from natural wolframite solid solutions, (Fe,Mn)WO₄, was obtained with synchrotron high-resolution powder X-ray diffraction (HRPXRD) data, Rietveld refinements, space group *P2/c*, and *Z* = 2. Wolframite solid solutions extend from ferberite (FeWO₄) to hübnerite (MnWO₄). The W and (Mn,Fe) cations are in six-fold coordination. This study shows that the unit-cell parameters, *a*, *b*, *c*, and β angle, vary linearly with the unit-cell volume, *V*, across the wolframite series. The average <Mn,Fe–O> distance increases linearly because of larger Mn²⁺ (0.83 Å) replacing smaller Fe²⁺ (0.78 Å) cations, whereas the average <W–O> distance increases slightly because of the higher effective charge of the smaller Fe²⁺ cation. The distortions of the two types of polyhedra across the series are discussed.

Keywords: wolframite solid solutions; structure; chemistry; synchrotron high-resolution powder X-ray diffraction (HRPXRD); Rietveld structure refinement



Citation: Umbsaar, D.A.; Antao, S.M. Structural Variations across Wolframite Solid Solutions, (Fe,Mn)WO₄. *Minerals* **2022**, *12*, 42. <https://doi.org/10.3390/min12010042>

Academic Editors: Nikita V. Chukanov and Ulf Hålenius

Received: 30 November 2021

Accepted: 22 December 2021

Published: 28 December 2021

Publisher's Note: MDPI stays neutral with regard to jurisdictional claims in published maps and institutional affiliations.



Copyright: © 2021 by the authors. Licensee MDPI, Basel, Switzerland. This article is an open access article distributed under the terms and conditions of the Creative Commons Attribution (CC BY) license (<https://creativecommons.org/licenses/by/4.0/>).

1. Introduction

Wolframite solid solutions extend from ferberite (FeWO₄) to hübnerite (MnWO₄). According to IMA CNMNC, wolframite with Fe > Mn is called ferberite and those with Mn > Fe is called hübnerite. Complete substitution occurs between Fe²⁺ and Mn²⁺ cations in wolframite, (Fe,Mn)WO₄. Hereafter, we use the name wolframite to cover the entire series between the two end members.

Tungstates and molybdates form two isostructural groups with the general formula MTO₄, where M is for divalent metal cations (M = Ca²⁺, Sr²⁺, Ba²⁺, Cd²⁺, and Pb²⁺) and T is for transition elements (T = W, Mo). The monoclinic wolframite-group minerals (space group *P2/c*) contain small divalent cations, such as Fe²⁺, Mn²⁺, Mg²⁺, Ni²⁺, and Co²⁺ in six-coordination with O atoms from six different octahedral WO₆ groups (Figure 1). The wolframite structure is based on W and (Fe,Mn) distorted octahedra forming infinite zig zag chains along the *c*-axis (Figure 1c). Each chain contains just one type of cation, and each octahedron is joined to the next by a common edge. Each W octahedral chain is attached by common corners to (Fe,Mn) chains, and each (Fe,Mn) chain is also surrounded by four W chains. The same types of octahedra are joined by edges and different types of octahedra are connected by corners.

The tetragonal scheelite-group minerals (space group *I4₁/a*) contain large divalent cations, such as Ca²⁺ and Pb²⁺, in eight-coordination with O atoms from eight different tetrahedral (WO₄)²⁻ and (MoO₄)²⁻ groups. The structure of scheelite is close to that of anhydrite, CaSO₄, and zircon, ZrSiO₄, but differs from these in the manner of linking of the CaO₈ polyhedra. The (WO₄)²⁻ and (MoO₄)²⁻ tetrahedra are flattened along the *c*-axis and join edges with CaO₈ or PbO₈ polyhedra in scheelite and wulfenite, respectively (these structures are not shown).

The problem of the O-atom coordinates in scheelite-type structure has been of interest in crystal chemistry for a long time [1]. These MTO₄ compounds contain W and Pb atoms with high atomic numbers that dominate the X-ray scattering process, so the light O-atom positions were not determined to a high precision. In addition, Pb atoms are good

absorbers of X-rays. Consequently, some authors choose neutrons instead of X-rays because the scattering amplitudes using neutrons are of the same order of magnitude for the atoms in these minerals.

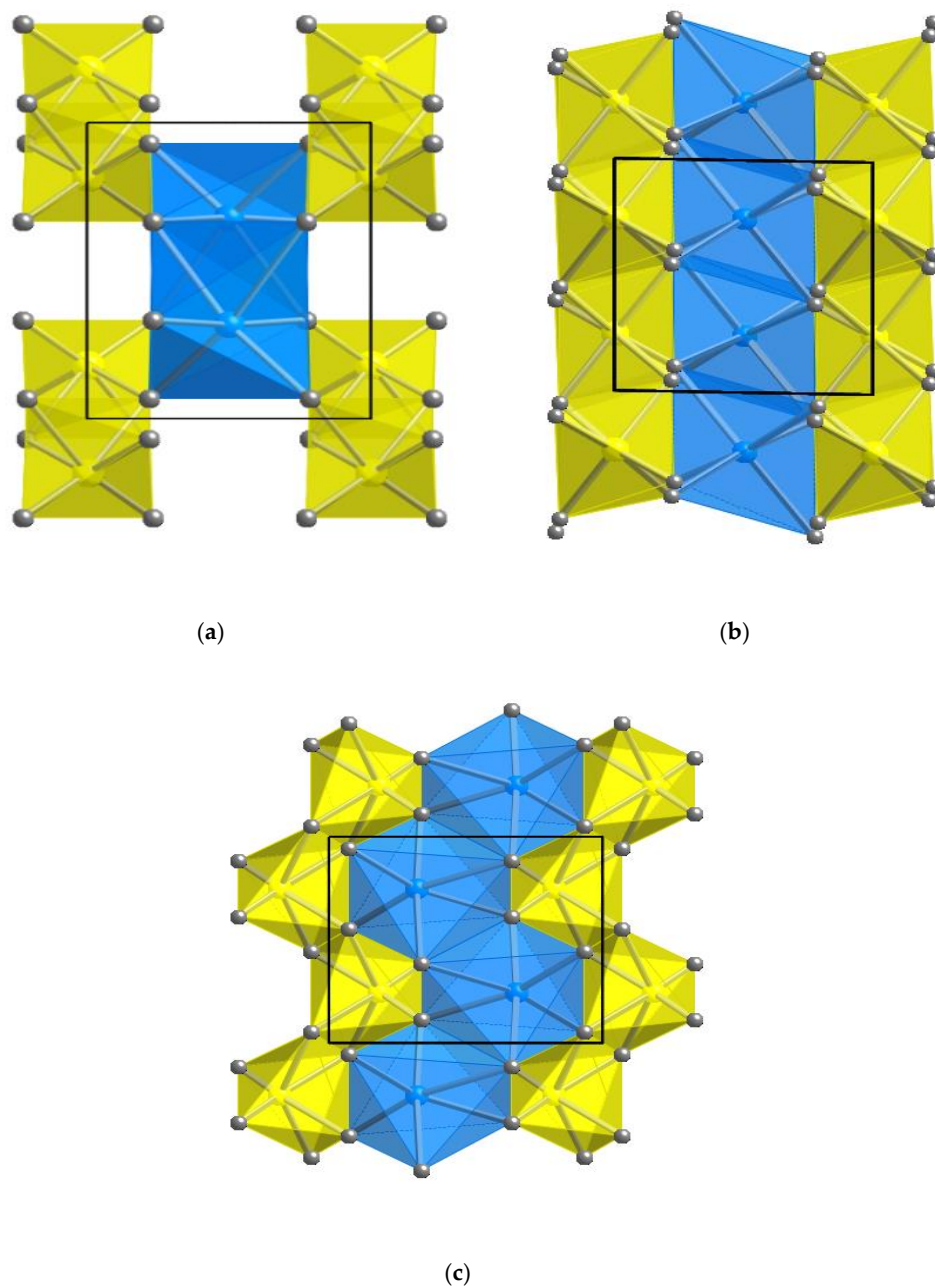


Figure 1. Structure of wolframite, $(\text{Fe,Mn})\text{WO}_4$, (space group $P2/c$) projected (a) down $[001]$ (**b**-axis is vertical and the **a**-axis is horizontal), (b) down $[010]$ (**c**-axis is vertical and the **a**-axis is horizontal), and (c) down $[100]$ (**c**-axis is vertical and the **b**-axis is horizontal). The O (grey spheres) oxygen atoms are indicated. The monoclinic unit-cell edges are outlined (black frame). The structure contains distorted WO_6 octahedra (yellow) and $(\text{Fe,Mn})\text{O}_6$ octahedra (blue) forming infinite zig-zag chains along the **c**-axis, as shown in (c).

The crystal structure of two similar ferberite samples from Liquinaste, Jujuy, Argentina is available [2,3] as well as another sample from Saxony, Germany [4]. The structure of a synthetic MnWO_4 sample is also known as well as its high-pressure behavior [5,6]. However, a complete picture of the structural variations across wolframite solid solutions

could not be deduced from the above studies, so the present study was carried out to fill this knowledge gap.

This study examines the structural variations across wolframite solid solutions based on the crystal structure of four natural samples that were obtained using synchrotron high-resolution powder X-ray diffraction (HRPXRD) data and Rietveld structure refinements. Some data from the literature are compared to the data from this study.

2. Experimental Methods

2.1. Electron-Probe Microanalysis (EPMA)

The wolframite samples were analyzed using a JEOL JXA-8200 WD-ED electron-probe microanalysis (EPMA). The samples were mounted in epoxy and polished for EPMA. The JEOL operating program on a Solaris platform was used for ZAF (atomic number, Z; absorption, A; fluorescence, F) correction and data reduction. The wavelength-dispersive (WD) analyses were conducted quantitatively using an accelerated voltage of 15 kV, a beam current of 20 nA, and a beam diameter of 5 μm . Relative analytical errors were 1% for major elements and 5% for minor elements. Various standards were used: chromite (Cr), pyromorphite (Pb), scheelite (W), CaMoO_4 (Ca, Mo), NiO (Ni), hornblende (Mg), ZnO (Zn), V_2O_5 (V), ilmenite (Fe, Ti), barite (S), and UC09059 hübnerite (Mn). Our four samples appeared to be homogeneous based on optical observations and EPMA analyses. Table 1 contains the average chemical composition from 10 spots for each sample. The localities of our four samples are given in Table 2. Based on EPMA and HRPXRD data, sample 1 contained two different phases with different compositions. The composition of two data points that may represent the two different phases are given in Table 1.

Table 1. Chemical compositions for four wolframite (Fe,Mn)WO₄ samples.

Oxides	Radii (Å) *	1a	1b	2	3	4
		wt. %				
MnO		15.14	20.07	17.66(29)	21.89(46)	23.41(12)
FeO		8.71	3.42	5.89(26)	1.51(56)	0.07(2)
ZnO		0.02	0.04	0.02(3)	0.01(1)	0.04(2)
MgO		0.02	0.00	0.00(2)	0.00(1)	0.00(1)
NiO		0.02	0.04	0.00(2)	0.03(2)	0.02(2)
CaO		0.00	0.00	0.00(1)	0.00(0)	0.00(0)
PbO		0.00	0.00	0.00(0)	0.00(0)	0.00(0)
WO ₃		76.11	76.00	76.47	76.29(16)	76.05(39)
MoO ₃		0.00	0.00	0.00(0)	0.00(0)	0.00(0)
SO ₃		0.06	0.21	0.26(8)	0.05(9)	0.08(11)
TiO ₂		0.02	0.00	0.00(5)	0.00(0)	0.01(1)
V ₂ O ₃		0.00	0.00	0.00(0)	0.00(0)	0.00(0)
Cr ₂ O ₃		0.01	0.00	0.00(1)	0.01(1)	0.00(1)
Total		100.11	99.78	100.30	99.79	99.68
Cations	-	apfu				
Mn ²⁺	0.83	0.645	0.856	0.748(12)	0.935(19)	1.000(5)
Fe ²⁺	0.78	0.367	0.144	0.247(11)	0.064(23)	0.003(1)
Zn ²⁺	0.74	0.001	0.001	0.001(1)	0.000(0)	0.002(1)
Mg ²⁺	0.72	0.001	0.000	0.000(1)	0.000(1)	0.000(1)
Ni ²⁺	0.69	0.001	0.001	0.000(1)	0.001(1)	0.001(1)
Ca ²⁺	1.00	0.000	0.000	0.000(0)	0.000(0)	0.000(0)
Pb ²⁺	1.19	0.000	0.000	0.000(0)	0.000(0)	0.000(0)
ΣA		1.015	1.002	0.996	1.000	1.006
W ⁶⁺	0.60	0.992	0.991	0.992(2)	0.998(3)	0.994(3)
Mo ⁶⁺	0.59	0.000	0.000	0.000(0)	0.000(0)	0.000(0)

Table 1. Cont.

Oxides	Radii (Å) *	1a	1b	2	3	4
S ⁶⁺	0.29	0.002	0.008	0.010(3)	0.002(3)	0.003(4)
Ti ⁴⁺	0.61	0.001	0.000	0.000(2)	0.000(0)	0.000(0)
V ³⁺	0.64	0.000	0.000	0.000(0)	0.000(0)	0.000(0)
Cr ³⁺	0.62	0.000	0.000	0.000(0)	0.000(0)	0.000(0)
ΣB		0.995	0.999	1.002	1.000	0.997
Σ(A + B)		2.010	2.001	1.998	2.000	2.003
% Hü		63.74	85.60	75.18	93.59	99.70

* Ionic radii are from Shannon [7]. The *apfu* are based on 4 oxygen atoms. % Hü = % hübnerite = [Mn/(Mn + Fe)] × 100. Sample 1 contains two similar phases, so 2 possible compositions are given from 2 data points, whereas the average composition from 10 data points is given for the other samples.

Table 2. Wolframite samples: locality, unit-cell parameters, and Rietveld refinement statistical indicators, R (F^2), χ^2 , etc.

No.	Localities	$a/\text{Å}$	$b/\text{Å}$	$c/\text{Å}$	$\beta/^\circ$	$V/\text{Å}^3$	* $R(F^2)$	χ^2	N_{obs}	N_{pts}	Var.
1a	Oregon Mine, Boulder, Colorado (VC758)	4.78219(4)	5.73389(4)	4.98336(3)	90.5631(6)	136.640(2)	0.0208	1.699	2134	43,067	43
1b	VC758	4.81212(3)	5.74991(4)	4.99266(3)	90.9304(6)	138.125(2)					
2	Tae Wha mine, Korea (VC315)	4.79440(2)	5.74073(2)	4.98734(2)	90.7109(3)	137.258(1)	0.0178	1.623	1065	43,067	28
3	Silverton, Colorado (VC692)	4.82435(2)	5.75627(2)	4.99611(1)	91.0773(2)	138.7188(8)	0.0271	3.664	983	41,444	28
4	Pasto Bueno, Peru (UC09059)	4.82991(2)	5.75974(2)	4.99795(2)	91.1475(2)	139.0101(9)	0.0238	2.791	1032	43,067	28

All samples were refined in space group $P2_1/c$ with $\lambda = 0.41279(2)$ Å. * $R(F^2) = R$ -structure factor based on observed and calculated structure amplitudes = $[\sum(F_o^2 - F_c^2)/\sum(F_o^2)]^{1/2}$. The 2θ range for each sample is from 2° to 45° . The values for N_{obs} (number of observed reflections), N_{pts} (number of data points), and Var. (number of variables) are given. Sample 1 contains two different phases. The weight % for phase-1a is 55.84(6) and phase-1b is 44.16(7).

2.2. Synchrotron High-Resolution Powder X-ray Diffraction (HRPXRD)

Single crystals of our wolframite samples, of about 0.2 mm in diameter, were hand-picked under a binocular microscope and finely ground in a corundum mortar and pestle for synchrotron high-resolution powder X-ray diffraction (HRPXRD) experiments that were performed at beamline 11-BM, Advanced Photon Source, Argonne National Laboratory. Each sample was loaded into a Kapton capillary (0.8 mm internal diameter) and rotated during the experiment at a rate of 90 rotations per second. The data were collected to a maximum 2θ of about 50° with a step size of 0.001° and a step time of 0.1 s per step. The HRPXRD traces were collected with a unique multi-analyzer detection assembly consisting of 12 independent silicon (111) crystal analyzers and LaCl_3 scintillation detectors that reduce the angular range to be scanned and allow for the rapid acquisition of data. A silicon (NIST 640c) and alumina (NIST 676a) standard (ratio of $1/3$ $\text{Si}_2/3$ Al_2O_3 by weight) was used to calibrate the instrument and to refine the monochromatic wavelength ($\lambda = 0.41279(2)$ Å) used in the experiment (Table 2). Additional details of the experimental set-up are given elsewhere [8–10]. The experimental techniques used in this study are well established [11–16].

2.3. Rietveld Structural Refinement

The crystal structure was modeled with the Rietveld method [17] that is incorporated in the GSAS program [18] and using the EXPGUI interface [19]. The starting atom coordinates, unit-cell parameters, and space group $P2_1/c$, $Z = 2$ were taken from Cid-Dresdner and Escobar [2]. The background was modeled with a Chebyshev polynomial (8 terms). The reflection-peak profiles were fitted using type-3 profile (pseudo-Voigt; [20,21]). The structure refinements were carried out by varying parameters in the following sequence: scale factor, background, unit-cell parameters, zero shift, profile, atom positions, and isotropic displacement parameters, U . The site-occupancy factor (*sofs*) for the Fe/Mn site is fixed based on EPMA values because these elements differ by just one electron. Finally, all variables were refined simultaneously. The $U(\text{O1})$ was set equal to $U(\text{O2})$. The *sofs* for the W and O sites were set equal to 1.

Table 2 contains unit-cell parameters and other information regarding data collection and refinement. Table 3 contains the atom coordinates and isotropic displacement parameters. Table 4 contains the bond distances. CIF files for the four samples are available as supplementary materials.

Table 3. Wolframite samples: atom coordinates and isotropic displacement parameters ($U \times 10^2 \text{ \AA}^2$).

Atom	-Site	1a	1b	2	3	4
Mn/Fe	<i>x</i>	$\frac{1}{2}$	$\frac{1}{2}$	$\frac{1}{2}$	$\frac{1}{2}$	$\frac{1}{2}$
	<i>y</i>	0.3202(2)	0.3149(3)	0.3181(1)	0.3139(1)	0.3131(1)
2 <i>f</i>	<i>z</i>	$\frac{3}{4}$	$\frac{3}{4}$	$\frac{3}{4}$	$\frac{3}{4}$	$\frac{3}{4}$
	<i>U</i>	0.29(1)	0.29(1)	0.31(1)	0.54(2)	0.31(1)
<i>sof</i>		0.65 Mn	0.86 Mn	0.75 Mn	0.94 Mn	1 Mn
		0.35 Fe	0.24 Fe	0.25 Fe	0.06 Fe	0 Fe
W	<i>x</i>	0	0	0	0	0
	<i>y</i>	0.17974(6)	0.18025(8)	0.17999(3)	0.17988(4)	0.17975(4)
2 <i>e</i>	<i>z</i>	$\frac{1}{4}$	$\frac{1}{4}$	$\frac{1}{4}$	$\frac{1}{4}$	$\frac{1}{4}$
	<i>U</i>	0.109(4)	0.109(4)	0.109(4)	0.323(4)	0.273(4)
O1	<i>x</i>	0.2149(6)	0.2084(7)	0.2139(3)	0.2137(4)	0.2136(4)
	<i>y</i>	−0.0980(5)	−0.1063(6)	−0.1032(3)	−0.0992(3)	−0.1035(3)
4 <i>g</i>	<i>z</i>	0.4433(7)	0.4351(8)	0.4396(4)	0.4392(4)	0.4458(4)
	<i>U</i>	0.07(3)	0.07(3)	0.05(3)	0.47(3)	0.25(5)
O2	<i>x</i>	0.2628(6)	0.2479(7)	0.2544(3)	0.2539(3)	0.2523(3)
	<i>y</i>	0.3655(5)	0.3766(6)	0.3702(3)	0.3730(3)	0.3680(3)
4 <i>g</i>	<i>z</i>	0.3972(7)	0.3880(8)	0.3945(4)	0.3893(4)	0.3952(4)

Space group $P2_1/c$, choice 1. The *sofs* for W, O1, and O2 were fixed at 1.0; and $U(O1) = U(O2)$.

Table 4. Bond distances (\AA) and polyhedral distortion indices for four wolframite samples.

Bond	1a	1b	2	3	4
(Fe,Mn)O ₆ octahedron					
Fe–O1 × 2	2.106(3)	2.074(3)	2.081(2)	2.093(2)	2.094(2)
Fe–O2 × 2	2.099(4)	2.189(4)	2.137(2)	2.166(2)	2.143(2)
Fe–O2 × 2	2.256(3)	2.263(3)	2.265(2)	2.274(2)	2.316(2)
<(Fe,Mn)–O> <6>	2.154	2.176	2.161	2.178	2.184
Average edge length	3.0239	3.0461	3.0306	3.0508	3.0590
Average angle	104.570	104.048	104.378	104.125	104.058
Polyhedral volume	12.9526	13.2503	13.0622	13.3194	13.4182
Octahedral angle variance	65.4243	83.6260	70.0429	78.6334	82.4303
Mean octahedral quadratic elongation	1.0199	1.0252	1.0212	1.0236	1.0255
WO ₆ octahedron					
W–O1 × 2	2.121(3)	2.132(4)	2.136(2)	2.122(2)	2.155(2)
W–O1 × 2	1.909(3)	1.926(4)	1.919(2)	1.936(2)	1.906(2)
W–O2 × 2	1.798(3)	1.773(4)	1.782(2)	1.786(2)	1.776(2)
<W–O> <6>	1.943	1.944	1.946	1.948	1.945
Average edge length	2.7145	2.7215	2.7222	2.7258	2.7218
Average angle	103.519	104.010	103.821	103.840	103.808
Polyhedral volume	9.2754	9.3836	9.3925	9.4119	9.3755
Octahedral angle variance	118.6792	97.5426	102.6663	104.9690	103.9077
Mean octahedral quadratic elongation	1.0407	1.0347	1.0363	1.0362	1.0377

3. Results and Discussion

3.1. Chemical Composition of Natural Wolframite Samples

The compositions of the wolframite samples are given in Table 1. The atom per formula unit (*apfu*) is based on four oxygen atoms. The W site is filled exclusively with W atoms. The divalent cation site is essentially filled with Mn and Fe atoms. All of our samples are Mn-rich with the % hübnerite $[(\text{Mn}/(\text{Mn} + \text{Fe})) \times 100]$ ranging from 64 to 100%.

Two possible compositions for phase-1a and phase-1b in sample 1 are given in Table 1. The X-ray diffraction data below show that sample 1 contains two separate phases that are slightly different from each other. These two phases differ in their Mn and Fe content. The Fe-rich phase-1a has a smaller unit-cell volume than the Mn-rich phase-1b, as expected, whereas sample 2 has values intermediate between phase-1a and phase-1b.

3.2. High-Resolution Powder X-ray Diffraction (HRPXRD) Traces for Natural Wolframite Samples

Except for sample 1, the traces for the other three samples contain sharp and symmetrical peaks with no impurity. An example for such a trace is shown for sample 2 that contains a single phase (Figure 2c,d). However, sample 1 contains two different phases as indicated by the split reflections (Figure 2a,b) compared to the un-split reflections in Figure 2c,d. These features are shown clearly in the expanded traces (Figure 2b,d). The crystal structure of both phases in sample 1 were obtained as well as their compositions (Tables 1 and 4). Splitting of reflections were observed in several other minerals [22–28].

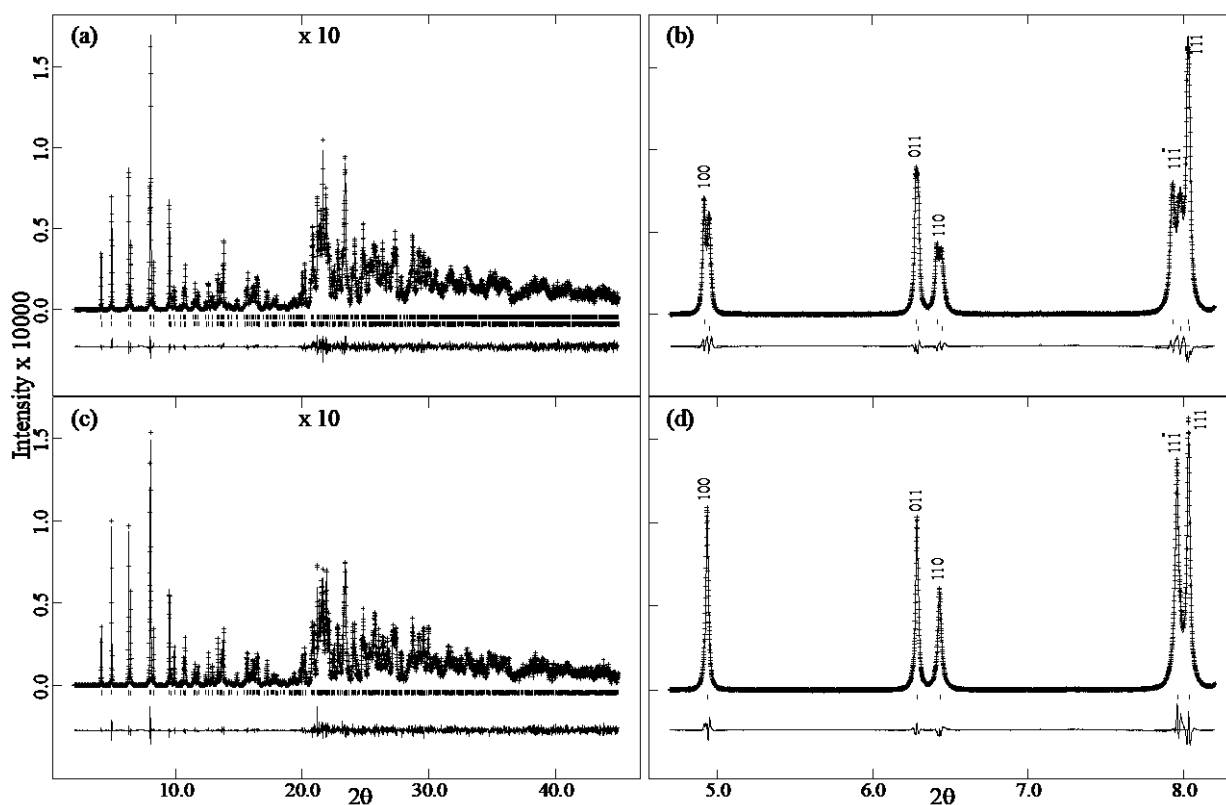


Figure 2. Comparison of HRPXRD traces for sample 1 (a,b) and sample 2 (c,d) together with the calculated (continuous line) and observed (crosses) profiles. The difference curve ($I_{obs} - I_{calc}$) with the same intensity scale is shown at the bottom of each trace. Short vertical lines indicate allowed reflection positions. The intensities for the trace and difference curve that are above 20° in 2θ are multiplied by 10 in both (a,c). Expanded traces are displayed in (b,d). The traces in (c,d) contain sharp and symmetrical peaks with no impurity peaks. Sample 1 contains two similar phases as indicated by the split reflections in (a,b) compared to the un-split reflections in (c,d).

3.3. Variations of the Unit-Cell Parameters across Wolframite, $(Fe,Mn)WO_4$, Solid Solutions

Across natural wolframite solid solutions, the unit-cell parameters a , b , c , and β with volume, V , vary linearly (Table 2, Figure 3). The a -axis (Figure 3a), b axis (Figure 3b), c -axis (Figure 3c), and β angle (Figure 3d) increase linearly with the increase in V . For comparison to our data, those from other studies are shown [3–5]. Based on the chemical analyses, the

substitution of larger Mn^{2+} (0.83 Å) occurs for smaller Fe^{2+} (0.78 Å) cations and causes the increase in unit-cell parameters with V .

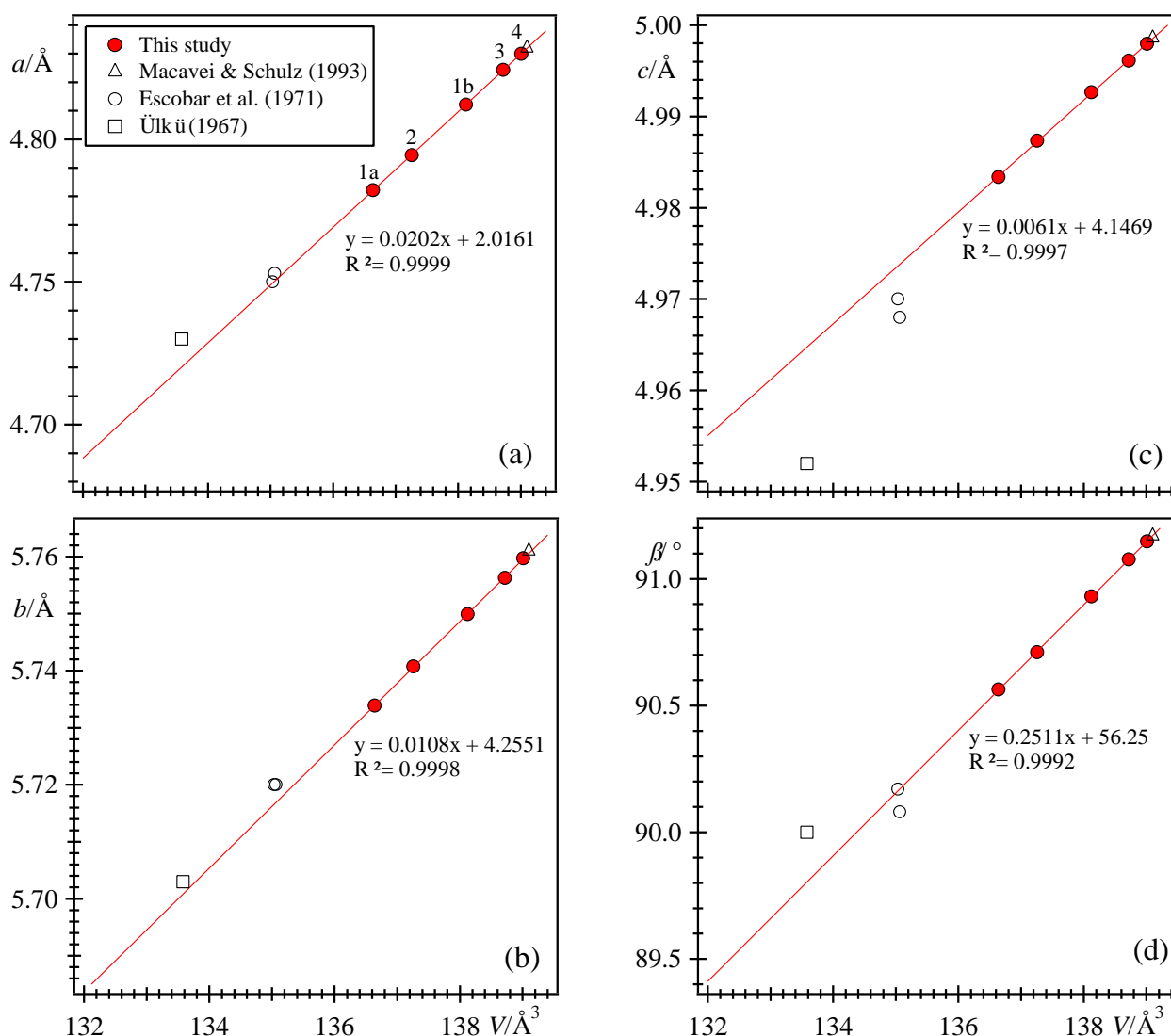


Figure 3. Variations of the unit-cell parameters (a) a , (b) b , (c) c , and (d) β with volume, V , across the wolframite series, $(\text{Fe,Mn})\text{WO}_4$. The literature data are from Macavei and Schulz [5] for a pure synthetic end member, MnWO_4 , Escobar et al. [3], and Ülkü [4]. The linear trend lines and equations are based only on data from this study. The unit-cell parameters increase with V across the series.

3.4. Variations of Structural Parameters across Wolframite, $(\text{Fe,Mn})\text{WO}_4$, Solid Solutions

The essential features of the wolframite structure obtained in this study are the same as those observed in previous studies. The wolframite structure consists of two main structural units: distorted $(\text{Fe,Mn})\text{O}_6$ and WO_6 octahedra (Figure 1). In our refinements of the wolframite structure, the site occupancy factors (*sofs*) for the Fe/Mn site were fixed by the EPMA data because these two elements differ by only one electron (Table 1). In fact, the Mn content varies linearly with the increase in unit-cell volume, V , as shown in Figure 4. It appears that a nearly pure natural FeWO_4 end member was studied by Ülkü [4] and a pure synthetic MnWO_4 end member was studied by Macavei and Schulz [5]. Based on our extrapolated data, it appears that the pure FeWO_4 may have a unit-cell volume of about 132 Å^3 . As such, the volume range were extended from 132 to about 139.4 Å^3 (Figures 3–5).

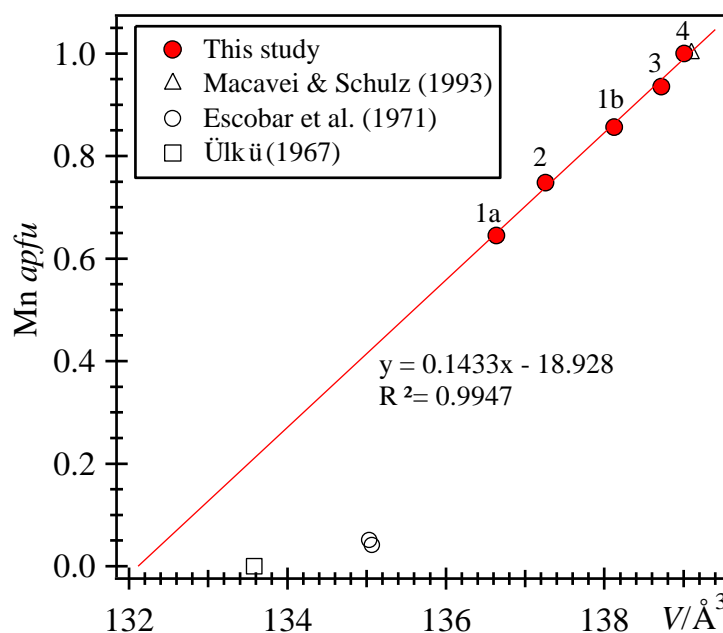


Figure 4. The Mn *apfu* varies linearly with the unit-cell volume, V . The inserted data points are from Macavei and Schulz [5] for a pure synthetic end member, MnWO_4 , Escobar et al. [3], and Ülkü [4].

The average $\langle\text{Fe,Mn}\text{--O}\rangle$ distance increases linearly with V and has values from about 2.154 (sample 1a) to 2.184 (sample 4), a difference of 0.030 Å (Table 4; Figure 5a). The average $\langle\text{W--O}\rangle$ distance increases linearly and has values from about 1.943 (sample 1a) to 1.948 (sample 3), a difference of 0.005 Å, which is about 6 times less than the difference for the average $\langle\text{Fe,Mn}\text{--O}\rangle$ distance (Figure 5b). The average $\langle\text{Fe,Mn}\text{--O}\rangle$ distance increases linearly because of the substitution of larger Mn^{2+} (0.83 Å) for smaller Fe^{2+} (0.78 Å) cations. End-member data from the literature [4,5] match the data from this study quite well (Figure 5a,b). However, the two similar data points from Escobar et al. [3] and Cid-Dresdner and Escobar [2] appear unreliable (see Figure 5).

Shannon [7] gives the following radii for atoms in six coordination in wolframite: $\text{Fe}^{2+} = 0.78$, $\text{Mn}^{2+} = 0.83$, $\text{W}^{6+} = 0.60$ Å, and three-coordination $\text{O}^{2-} = 1.36$ Å, so the radii sum gives $\text{Fe--O} = 2.14$ Å, which is close to the projected average $\langle\text{Fe--O}\rangle = 2.095$ Å (Figure 5a). The radii sum gives $\text{Mn--O} = 2.19$ Å, which is close to the average $\langle\text{Mn--O}\rangle = 2.184$ Å in sample 4. In addition, the radii sum gives $\text{W--O} = 1.96$ Å, which is close to the average $\langle\text{W--O}\rangle = 1.948$ Å in sample 3 (Table 4). In danalite, $\text{Fe}_8[\text{Be}_6\text{Si}_6\text{O}_{24}]\text{S}_2$, the average $\langle\text{Fe--O}\rangle_{\langle 3 \rangle}$ distance is 2.033(3) Å [29], whereas in magnesioferrite spinel, MgFe_2O_4 , the average $\langle\text{Fe--O}\rangle_{\langle 6 \rangle}$ distance is 2.061(1) [30]. The values are similar to those for the Fe end-member of wolframite.

The distortion indices of the W and (Fe,Mn) polyhedra are given in Table 4. Among our samples, sample 1b has an intermediate composition and contains the shortest Fe–O1 and W–O2 distances. However, the average $\langle\text{Fe,Mn}\text{--O}\rangle$ distance is comparable to those in the other samples as indicated in Figure 5a. The distortion indices across the series represent the data quite well (Figure 6), especially those in Figure 6a,d. Because sample 1b is about 44 wt. %, the refinement results may not be as accurate as for the other samples, including sample 1a. However, the possibility of some Fe^{3+} and vacancies replacing Fe^{2+} cannot be ruled out.

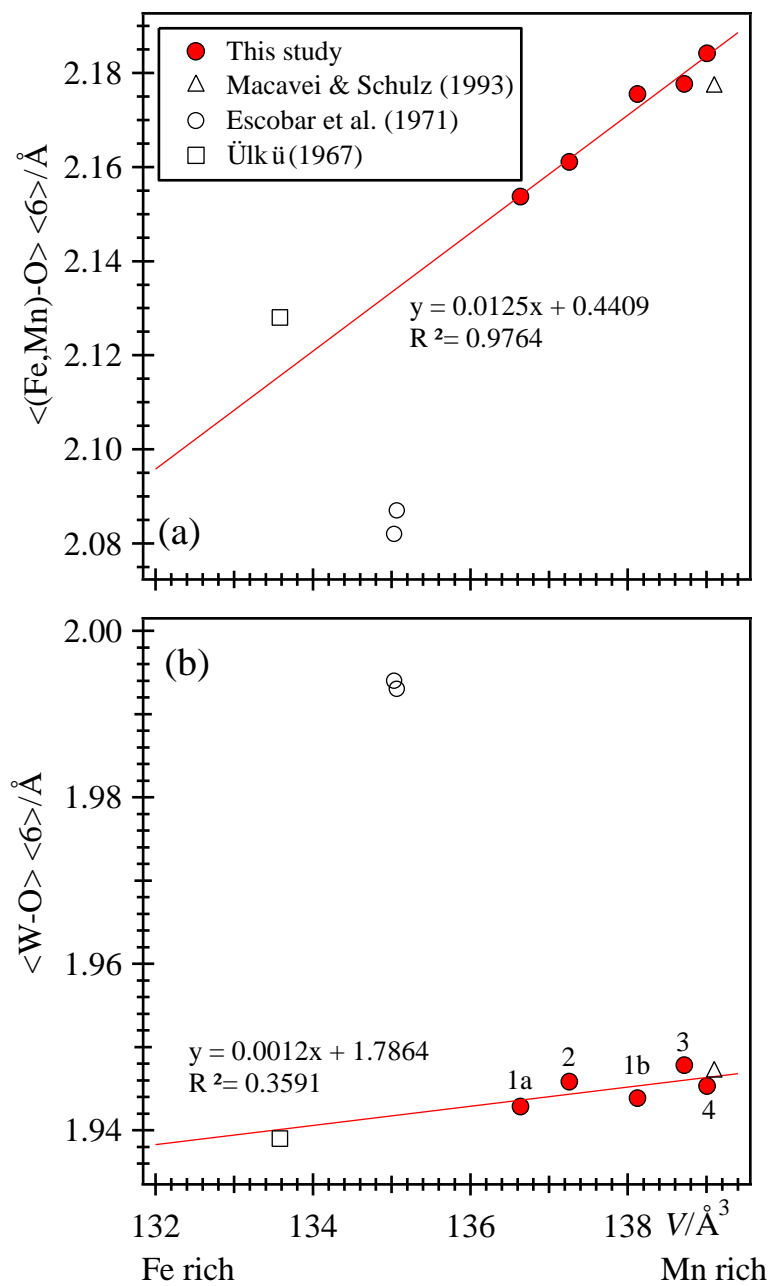


Figure 5. Structural variations across the wolframite series with increasing V : (a) the average $\langle \text{Fe,Mn}-\text{O} \rangle$ distance increases linearly because of Mn^{2+} (0.83 \AA) replacing Fe^{2+} (0.78 \AA) cations. (b) The average $\langle \text{W}-\text{O} \rangle$ distance increases slightly with V because Mn^{2+} has a less effective polarizing power to the O atoms than the smaller Fe^{2+} cation. The data from Escobar et al. [3] appear to be unreliable because they are far away from the red trend lines.

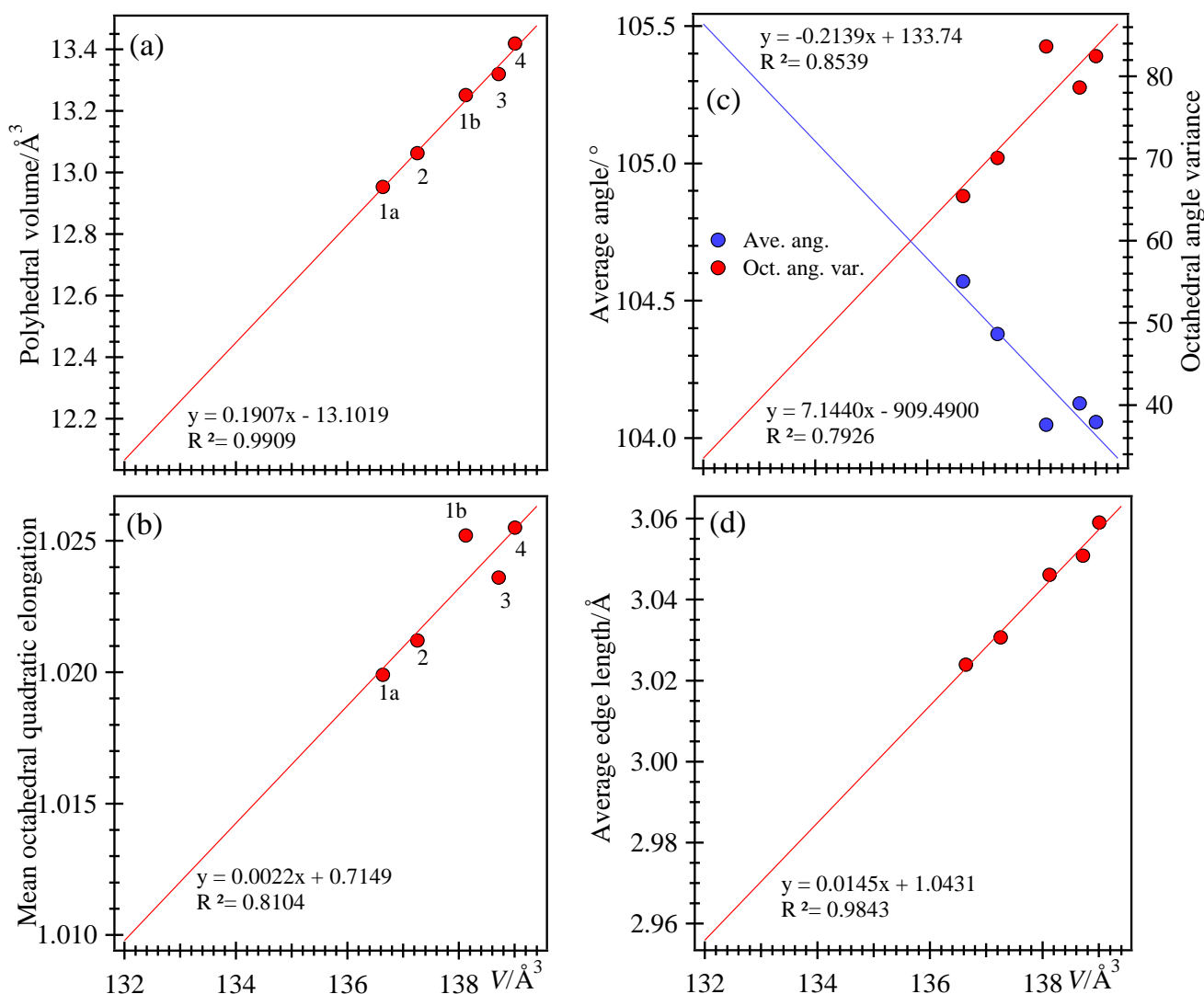


Figure 6. $(\text{Fe,Mn})\text{O}_6$ polyhedral distortion indices across the wolframite series with increasing V : All the trend lines appear to represent variations across the series quite well. However, those in (a) and (d) have the highest correlation factors, but the values are lower in (b,c).

4. Concluding Remarks

Understanding $(\text{Fe,Mn})\text{WO}_4$ solid solutions requires good structural data across the series. Although a few single-crystal structure refinements are available for a few members across the series, it was not possible to examine the structural variations across the series using those studies. This study shows that good structural information can be obtained with synchrotron HRPXRD data and the Rietveld refinement method to show expected linear systematic variations across wolframite solid solutions. The unit-cell parameters, a , b , c , and β angle vary linearly with the unit-cell volume, V . The average $\langle \text{W-O} \rangle$ distance increases slightly with the increase in V from ferberite to hübnerite because of the higher effective charge of the smaller Fe^{2+} cation. The average $\langle \text{Mn,Fe-O} \rangle$ distance increases linearly with V because of the larger Mn^{2+} (0.83 Å) replacing the smaller Fe^{2+} (0.78 Å) cations.

Supplementary Materials: CIF files for the four samples are available online at <https://www.mdpi.com/article/10.3390/min12010042/s1>.

Author Contributions: The academic editor and three anonymous reviewers are thanked for comments that helped to improve this manuscript. D.A.U. performed the EPMA experiment and analyzed the chemical composition data. S.M.A. conceived the project and analyzed the HRPXRD data. Both authors contributed to writing and editing the manuscript. All authors have read and agreed to the published version of the manuscript.

Funding: This research was funded by a NSERC Discovery Grant to SMA, grant number 10013896.

Acknowledgments: Robert Marr is thanked for his help with the EPMA analysis. The HRPXRD data were collected at the X-ray Operations and Research beamline 11-BM, Advanced Photon Source (APS), Argonne National Laboratory (ANL). Use of the APS was supported by the U.S. Dept. of Energy, Office of Science, Office of Basic Energy Sciences, under Contract No. DE-AC02-06CH11357.

Conflicts of Interest: The authors declare no conflict of interest.

References

1. Vegard, L. Results of crystal analysis. In *Space Lattices and Atomic Dimensions*; I Kommission hos J. Dybwad: Oslo, Norway, 1925.
2. Cid-Dresdner, H.; Escobar, C. The crystal structure of ferberite, FeWO_4 . *Z. Krist.* **1968**, *127*, 61–72. [[CrossRef](#)]
3. Escobar, C.; Cid-Dresdner, H.; Kittl, P.; Dümler, I. The relation between “light wolframite” and common wolframite. *Am. Mineral.* **1971**, *56*, 489–498.
4. Ülkü, D. Untersuchungen zur Kristallstruktur und magnetischen Struktur des Ferberits FeWO_4 . *Z. Krist.* **1967**, *124*, 192–219. [[CrossRef](#)]
5. Macavei, J.; Schulz, H. The crystal structure of wolframite type tungstates at high pressure. *Z. Krist.* **1993**, *207*, 193–208.
6. Errandonea, D.; Ruiz-Fuertes, J. A brief review of the effects of pressure on wolframite-type oxides. *Crystals* **2018**, *8*, 71. [[CrossRef](#)]
7. Shannon, R.D. Revised effective ionic radii and systematic studies of interatomic distances in halides and chalcogenides. *Acta Crystallogr.* **1976**, *A32*, 751–767. [[CrossRef](#)]
8. Lee, P.L.; Shu, D.; Ramanathan, M.; Preissner, C.; Wang, J.; Beno, M.A.; Von Dreele, R.B.; Ribaud, L.; Kurtz, C.; Antao, S.M.; et al. A twelve-analyzer detector system for high-resolution powder diffraction. *J. Synchrotron Radiat.* **2008**, *15*, 427–432. [[CrossRef](#)]
9. Wang, J.; Toby, B.H.; Lee, P.L.; Ribaud, L.; Antao, S.M.; Kurtz, C.; Ramanathan, M.; Von Dreele, R.B.; Beno, M.A. A dedicated powder diffraction beamline at the advanced photon source: Commissioning and early operational results. *Rev. Sci. Instrum.* **2008**, *79*, 85105. [[CrossRef](#)]
10. Antao, S.M.; Hassan, I.; Wang, J.; Lee, P.L.; Toby, B.H. State-of-the-art high-resolution powder X-ray diffraction (HRPXRD) illustrated with Rietveld structure refinement of quartz, sodalite, tremolite, and meionite. *Can. Mineral.* **2008**, *46*, 1501–1509. [[CrossRef](#)]
11. Antao, S.M. Crystal-structure analysis of four mineral samples of anhydrite, CaSO_4 , using synchrotron high-resolution powder X-ray diffraction data. *Powder Diffr.* **2011**, *26*, 326–330. [[CrossRef](#)]
12. Parise, J.B.; Antao, S.M.; Michel, F.M.; Martin, C.D.; Chupas, P.J.; Shastri, S.; Lee, P.L. Quantitative high-pressure pair distribution function analysis. *J. Synchrotron Radiat.* **2005**, *12*, 554–559. [[CrossRef](#)]
13. Hassan, I.; Antao, S.M.; Parise, J.B. Häuyne: Phase transition and high-temperature structures obtained from synchrotron radiation and Rietveld refinements. *Mineral. Mag.* **2004**, *68*, 499–513. [[CrossRef](#)]
14. Hassan, I.; Antao, S.M.; Hersi, A.A. Single-crystal XRD, TEM, and thermal studies of the satellite reflections in nepheline. *Can. Mineral.* **2003**, *41*, 759–783. [[CrossRef](#)]
15. Antao, S.M.; Hassan, I.; Mulder, W.H.; Lee, P.L. The $R\text{-}3c \rightarrow R\text{-}3m$ transition in nitratine, NaNO_3 , and implications for calcite, CaCO_3 . *Phys. Chem. Miner.* **2008**, *35*, 545–557. [[CrossRef](#)]
16. Zaman, M.; Schubert, M.; Antao, S. Elevated radionuclide concentrations in heavy mineral-rich beach sands in the Cox’s Bazar region, Bangladesh and related possible radiological effects. *Isot. Environ. Health Stud.* **2012**, *48*, 512–525. [[CrossRef](#)]
17. Rietveld, H.M. A profile refinement method for nuclear and magnetic structures. *J. Appl. Crystallogr.* **1969**, *2*, 65–71. [[CrossRef](#)]
18. Larson, A.C.; Von Dreele, R.B. *General Structure Analysis System (GSAS)*; Los Alamos National Laboratory Report, LAUR 86-748; Los Alamos National Laboratory: Los Alamos, NM, USA, 2000.
19. Toby, B.H. EXPGUI, a graphical user interface for GSAS. *J. Appl. Crystallogr.* **2001**, *34*, 210–213. [[CrossRef](#)]
20. Cagliotti, G.; Paoletti, A.; Ricci, F.P. Choice of collimators for a crystal spectrometer for neutron diffraction. *Nucl. Instrum.* **1958**, *3*, 223–228. [[CrossRef](#)]
21. Thompson, P.; Cox, D.E.; Hastings, J.B. Rietveld refinement of Debye-Scherrer synchrotron X-ray data from alumina. *J. Appl. Crystallogr.* **1987**, *20*, 79–83. [[CrossRef](#)]
22. Antao, S.M. Is near-endmember birefringent grossular non-cubic? New evidence from synchrotron diffraction. *Can. Mineral.* **2013**, *51*, 771–784. [[CrossRef](#)]
23. Antao, S.M. The mystery of birefringent garnet: Is the symmetry lower than cubic? *Powder Diffr.* **2013**, *28*, 281–288. [[CrossRef](#)]
24. Antao, S.M.; Hassan, I. A two-phase intergrowth of genthelvite from Mont Saint-Hilaire, Quebec. *Can. Mineral.* **2010**, *48*, 1217–1223. [[CrossRef](#)]

25. Antao, S.M.; Klincker, A.M. Crystal structure of a birefringent andradite-grossular from Crowsnest Pass, Alberta, Canada. *Powder Diffr.* **2014**, *29*, 20–27. [[CrossRef](#)]
26. Antao, S.M.; Mohib, S.; Zaman, M.; Marr, R.A. Ti-rich andradites: Chemistry, structure, multi-phases, optical anisotropy, and oscillatory zoning. *Can. Mineral.* **2015**, *53*, 133–158. [[CrossRef](#)]
27. Antao, S.M. Crystal structure of morimotoite from Ice River, Canada. *Powder Diffr.* **2014**, *29*, 325–330. [[CrossRef](#)]
28. Antao, S.M.; Round, S.A. Crystal chemistry of birefringent spessartine. *Powder Diffr.* **2014**, *29*, 233–240. [[CrossRef](#)]
29. Antao, S.M.; Hassan, I.; Parise, J.B. The structure of danalite at high temperature obtained from synchrotron radiation and Rietveld refinements. *Can. Mineral.* **2003**, *41*, 1413–1422. [[CrossRef](#)]
30. Antao, S.M.; Hassan, I.; Parise, J.B. Cation ordering in magnesioferrite, MgFe_2O_4 , to 982 °C using in situ synchrotron X-ray powder diffraction. *Am. Mineral.* **2005**, *90*, 219–228. [[CrossRef](#)]